Numerical Investigation of Constraint Effects on Fatigue Crack Propagation

I. Varfolomeev and S. Moroz

Fraunhofer Institute for Mechanics of Materials IWM,
Wöhlerstr. 11, 79111 Freiburg, Germany
igor.varfolomeyev@iwm.fraunhofer.de
sergii.moroz@iwm.fraunhofer.de

ABSTRACT. *The paper presents results of numerical modelling of elastic-plastic stress and strain fields at the tip of a propagating crack under cyclic loading. A particular motivation is to investigate the difference in fatigue crack growth rates previously observed in tests on M(T) and C(T) specimens made of 25CrMo4 (EA4T) steel. The stress field triaxiality (constraint) is considered as a factor influencing the deformation and, accordingly, closure behaviour at the crack tip. Among numerical issues studied in the paper are the strain hardening behaviour, consideration of the crack face contact, definition of the onset of crack opening, possible simplifications of numerical modelling by using the boundary layer formulation. The numerical results suggest that, using the effective stress intensity factor range, a reasonable explanation to the experimental findings can be provided.*

INTRODUCTION

Plasticity induced crack closure is widely acknowledged as a phenomenon affecting fatigue crack behaviour in metallic materials [1]. Especially in the near threshold regime as well as under variable amplitude loading, the crack closure can considerably influence crack propagation rates. Depending on the material strain hardening, crack and component geometry, the level and sequence of applied loading, crack acceleration or retardation effects may become significant, and an additional effort is then required to transfer fatigue crack growth properties from standard test specimens to describe the component behaviour.

To account for the plasticity induced crack closure, several analytical models have been derived and implemented in computer codes, see e.g. [2-5]. Most of them are based on approximate estimates of the plastic zone size ahead of the crack tip. As this is dependent, among other factors, on the triaxiality of the stress state (crack tip constraint), fatigue crack growth behaviour is affected by the geometry of a cracked specimen or component, respectively, as well as by loading conditions. In principal, this matter can be taken into account in existing models [2,5,6] by applying appropriate, geometry dependent solutions for stress intensity factors and related constraint

parameters, though certain model calibration is necessary [6]. Another approach is based on a numerical simulation of elastic-plastic crack tip fields under relevant loading conditions [7-10]. Despite of the complexity and costs associated with detailed numerical analyses, this way allows for essential deformation phenomena to be explored and included in simplified engineering models.

This study is motivated by some experimental results previously derived in [11-12]. These include fatigue crack growth measurements on various specimen geometries made of 25CrMo4 (EA4T) steel widely used in the manufacturing of railway axles. In particular, a considerable difference in fatigue crack growth rates was observed for standard specimens of types M(T) and C(T). Further verification tests performed on round bars with semi-elliptical cracks, considered to be representative of the crack propagation in component like specimens, revealed additional uncertainties regarding the transferability of material data to the component assessment.

To explore the possibility of an analytical description of those effects, a numerical analysis is applied below to simulate crack growth behaviour for the M(T) and C(T) specimen geometries with a special attention given to model plasticity induced crack closure. In particular, the analysis results suggest an adequate description of the crack growth rates for different specimens taking account of the crack closure. Various definitions of the crack opening stress intensity factor are discussed and applied to derive a correlation between the experimentally measured crack growth rates and calculated effective stress intensity ranges. Furthermore, two different approaches to simulate the crack growth behaviour – via modelling the entire specimens and by applying the boundary layer formulation – are considered and the respective results are discussed.

REVIEW OF FATIGUE CRACK GROWTH DATA FOR EA4T

Fatigue crack growth rates for the EA4T steel were experimentally derived in [11,12] at two stress ratios R = -1 and 0.1, thus covering a large part of the R range typical for loading conditions in railway axles. Mainly M(T) specimens with the cross-section 10×24 mm² were employed in [11,12], as these allow for fatigue crack growth measurements both in tensile and compressive load regimes. While the value R = -1 is representative for the cylindrical shaft subjected to rotary bending, stress ratios up to some 0.5 may arise when assessing the crack propagation at locations near press fittings, where the cyclic bending stress is superimposed with residual stresses due to press fitting. Note that the stress ratio in the latter case may vary within a rather broad range, depending on the stress amplitudes in the associated load spectrum.

Figure 1 shows experimental data from [12] related to the stress ration R = 0.1. Besides M(T), a C(T)-25 standard specimen geometry was investigated. Additionally, three specimens containing semi-elliptical surface cracks – two round bars with the diameter of 50 mm (BP1, BP2) and a flat plate with the cross-section 30×140 mm² (BP3), all subjected to plane bending with R = 0.1, were used in verification tests. As the M(T) and C(T) results show certain scatter, the related data points are approximated

by the NASGRO type equation [4], plotted as two curves in Fig. 1. The crack growth rates in the round bars were evaluated for the depth direction of the semi-elliptical crack, the results for the flat plate are given for both the depth and the length directions.

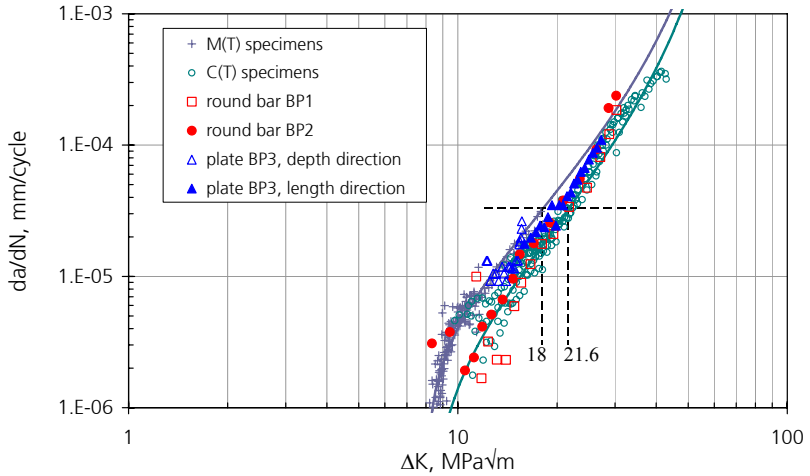

Figure 1. Fatigue crack growth rates for EA4T material measured on different specimens.

Apparently, there is a considerable discrepancy between the mean curves for different specimens. Both the data scatter and difference between the mean curves increase with approaching the fatigue threshold region. Though the M(T) curves seem to provide a conservative description for the propagation behaviour of surface cracks, further investigations are useful to explore the geometry effects and include these in analytical crack growth models.

NUMERICAL APPROACH

The numerical study performed in this paper is focused on the different crack growth behaviour for M(T) and C(T) specimens. To minimize the analysis extent and obtain possibly realistic predictions of the evolution of crack tip fields at cyclic loading, the middle range of the fatigue crack growth curve is investigated. In doing so, the numerical calculations are performed assuming the crack propagation rate of 3.3×10^{-5} mm/cycle, at cyclic loading with $R = 0.1$ and the stress intensity factor ranges of about $\Delta K = 18$ MPa√m for the M(T) specimen and 21.6 MPa√m for the C(T) specimen, as indicated in Fig. 1.

The finite-element (FE) models employed in this study are shown in Fig. 2. These represent both the whole specimen geometries (half-specimen for the M(T) configuration) and their approximation by a boundary layer model (BLM). In the BLM formulation, the boundary conditions are prescribed via nodal tractions applied to the model boundary based on the stress intensity factor and the T-stress values for the

respective specimen configuration. In all cases, the contact between the opposite crack faces is considered. Furthermore, plane strain conditions are assumed.

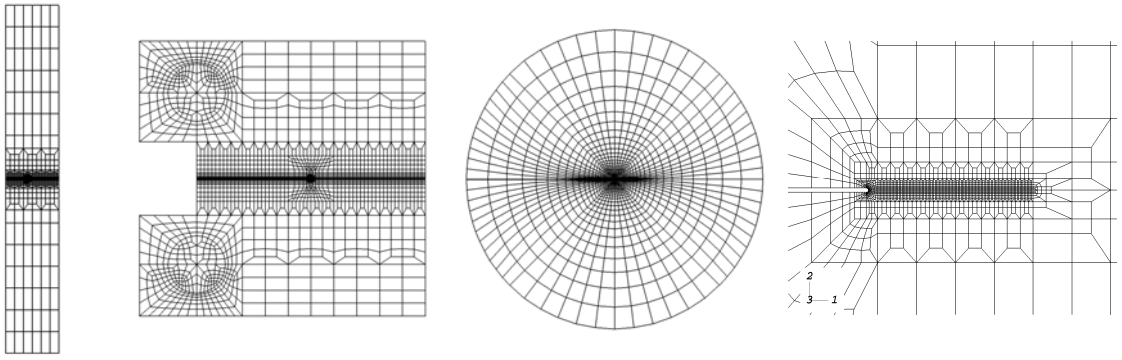

Figure 2. Finite-element models: a) M(T) specimen, half-model; b) C(T) specimen; c) boundary layer model; d) details of the crack tip region.

The same topology of the crack tip region is used in all models (Fig. 2d). The crack originates at an initial notch with the tip radius of 3 μm and propagates along the symmetry plane. The total crack extension modelled in the analyses is 0.2 mm. The corresponding fine mesh region consists of 100 equally spaced elements with the element length of 2 μm. The crack extension is simulated by a consecutive release of nodes in the ligament that belong to the upper and lower halves of the model and are initially connected via multi-point constraints. To achieve the crack growth rate of 3.3×10^{-5} mm/cycle, the node release at the current crack tip is performed after applying 60 load cycles.

The numerical calculations were carried out using the ABAQUS FE code [13]. The combined kinematic and isotropic cyclic strain hardening model implemented in [13] was employed. The corresponding cyclic stress versus strain curve is shown in Fig. 3 together with experimental data reported in [14].

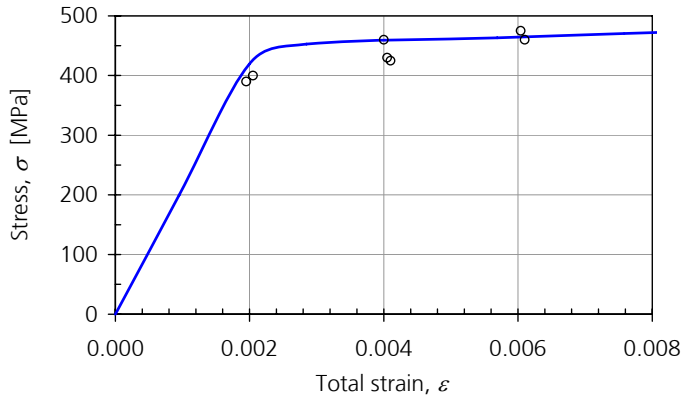

Figure 3. Cyclic stress-strain curve for EA4T: experimental data [16] and their analytical approximation (curve).

RESULTS

Full Model versus BLM

The BLM formulation is a promising approach that can be applied to various cracked geometries, including surface cracks, to minimize the computational effort, see e.g. [7]. Figure 4 compares the stress and strain components, σ_{22} and ε_{22}, acting normal to the crack propagation direction in the ligament, for the initial stationary crack subjected to monotonic loading with K_{max} = 20 and 24 MPa$\sqrt{m}$ for the M(T) and C(T) specimens, respectively. Except for slightly different strain distributions near the crack tip in the M(T) specimen, the agreement between the solutions for the full models and BLM is fairly good.

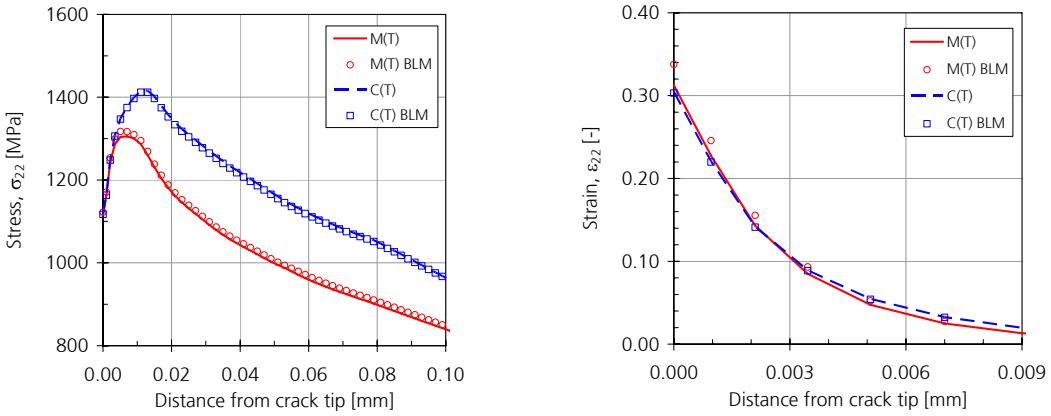

Figure 4. Stress and strain distributions ahead of a stationary crack tip in M(T) and C(T) specimens, monotonic loading.

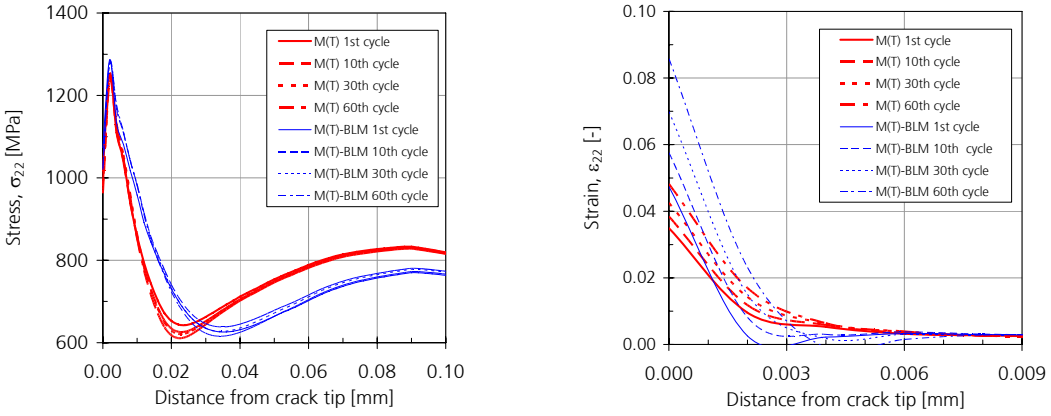

Figure 5. Stress and strain distributions ahead of a growing crack tip in M(T) specimen, cyclic loading.

However, the above conclusion does not hold for a crack propagating under cyclic loading. For the M(T) specimen, Fig. 5 demonstrates increasing deviation between the full specimen and BLM solutions with increasing number of cycles. Possible

explanations for this behaviour are the effect of higher order non-singular elastic terms on the plastic deformation at the crack tip, as well as cyclic strain hardening.

Therefore, caution is advised when applying the BLM formulation to problems where high load cycles and propagating cracks are to be considered. For this reason, further calculations in this paper are based on the use of full specimen models.

Crack Opening at Cyclic Loading

Figure 6 presents crack opening profiles for the M(T) and C(T) specimens for an intermediate crack length, at different levels of applied loading scaled with respect to the maximum load in the cycle. Accordingly, the two geometries reveal rather different crack opening behaviour. Both cracks remain closed for at least 50% of the load cycle. At 65% of the maximum load the crack in the M(T) specimen is completely, while that in the C(T) specimen partly open: namely, some portion of the crack faces for the C(T) still remains in contact, thus reducing the effective crack driving force.

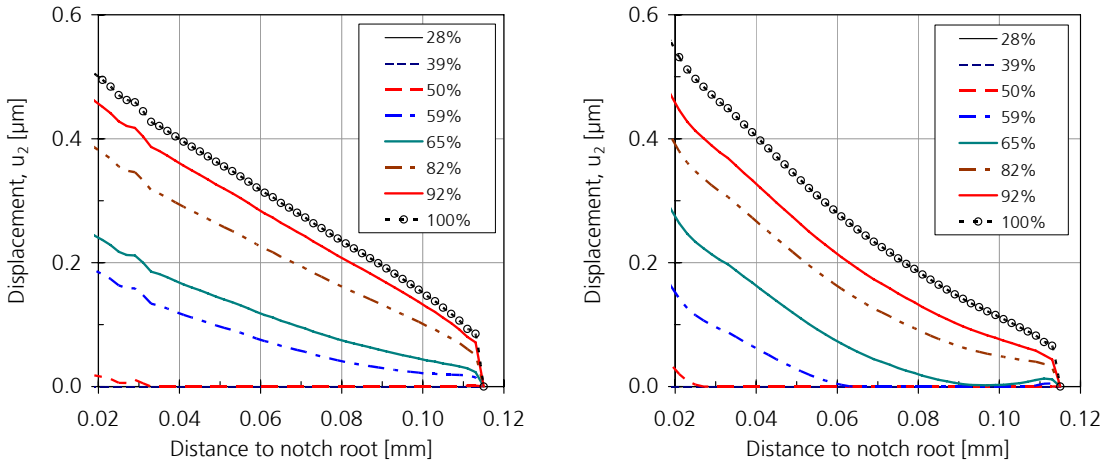

Figure 6. Crack opening profiles for M(T) (left) and C(T) (right) specimens.

A more detailed comparison of the both specimen geometries is given in Fig. 7 that shows the crack tip opening displacement (CTOD), i.e. the displacement for the node next to the crack tip. These results allow for an approximate evaluation of the effective stress intensity factor range. The latter is normally defined as

$$\Delta K_{eff} = K_{\max} - K_{op}$$

from the linear-elastic stress intensity factors at maximum loading and at the onset of crack opening. Based on the curves in Fig. 7, the crack tip opening for the M(T) and C(T) specimens is achieved at some 55% and 62% of the maximum load, or at K_{op} = 11 and 14.9 MPa√m, respectively. This yields ΔK_{eff} = 9 MPa√m for the M(T) specimen and ΔK_{eff} = 9.1 MPa√m for the C(T) specimen, thus suggesting nearly equal crack growth rates for both crack geometries.

The above result is also consistent with the assumption that the crack growth rate is governed by the CTOD range. According to Fig. 7, the latter constitutes similar values of 0.117 mm and 0.132 mm for the M(T) and C(T) specimens, respectively.

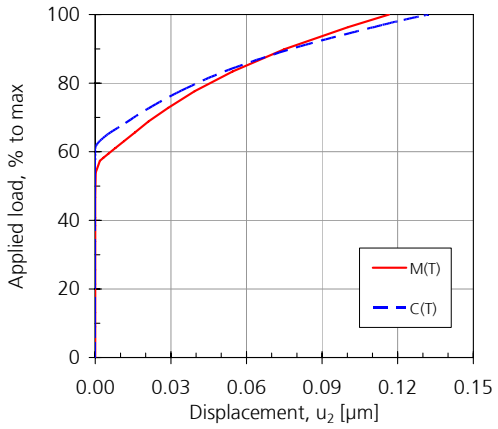

Figure 7. CTOD versus the fraction of maximum load in a cycle.

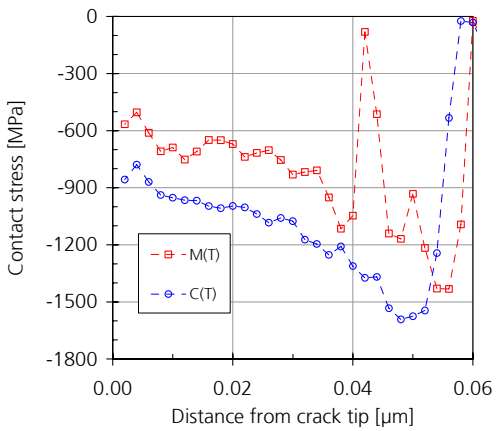

Figure 8. Contact stress along the crack face at minimum load in a cycle.

Crack Contact Stresses

Instead of evaluating the crack opening load based on nodal displacements, a contact stress method is utilized in [9]. Accordingly, the applied range ΔK is reduced by a value that is necessary to compensate the negative stress intensity factor due to the contact stresses. Potential limitations of such an approach result from the assumed linear-elastic superposition of the stress intensity factors due to external and contact loads, as this is strictly not applicable in the presence of the contact interaction and crack tip plasticity. Moreover, an accurate calculation of crack contact forces may become rather problematic. Nevertheless, the approach [9] is employed below for comparison purposes.

Figure 8 shows computed contact stresses along the crack faces in M(T) and C(T) specimens upon a crack extension of 0.06 mm (30 elements) from the initial notch, at the minimum load level. Due to a final radius of the initial notch root, the notch surfaces remain free of contact interaction. Certain numerical inaccuracies can be mentioned at the early stage of crack growth in the M(T) specimen, resulting is the oscillating contact stresses. Using the computed contact stresses along with the weight functions for the considered specimen geometries [15], the stress intensity factors required to compensate the crack contact forces are found to be 8.8 MPa$\sqrt{m}$ for the M(T) and 11.8 MPa$\sqrt{m}$ for the C(T) specimens. Then the effective stress intensity factor ranges become ΔK_{eff} = 9.2 MPa$\sqrt{m}$ and ΔK_{eff} = 9.8 MPa$\sqrt{m}$, respectively. Though these are somewhat higher than the corresponding values estimated from the crack opening profiles, the contact stress approach seems to yield consistent results.

CONCLUSIONS

Elastic-plastic analyses of crack tip fields performed in this study give a reasonable explanation for the difference in fatigue crack growth rates observed in tests on the EA4T steel using M(T) and C(T) specimens. In particular, the results suggest that the

effective stress intensity factor range concept provides a proper measure of the crack driving force for specimens with different crack tip constraints. Though somewhat different values of ΔK_{eff} are derived based on the crack opening displacement and the crack contact stress methods, both results series are consistent yielding close ΔK_{eff} values for the M(T) and C(T) geometries at equal crack growth rates.

Reservations should be made due to two-dimensional FE models adopted in this study, so that further analysis effort is required to explore specific effects for surface cracks. In this context the boundary layer model seems to have a limited applicability with respect to its ability of describing fatigue crack propagation in elastic-plastic materials.

REFERENCES

1. Elber, W. (1970) *Eng. Fract. Mech*. **2**, 37-45.
2. Newman, J.C., Jr. (1981). In: *Methods and Models for Predicting Fatigue Crack Growth under Random Loading*, ASTM STP 748, J.B. Chang and C.M. Hudson (Eds.), American Society for Testing and Materials, Philadelphia, pp. 53-84.
3. Newman, J.C., Jr. (1984) *Int. J. Fracture* **24**, R131-R135.
4. Fatigue Crack Growth Computer Program „NASGRO“ Version 3.0 – Reference Manual, National Aeronautics and Space Administration (NASA), JSC-22267B, 2000
5. Liu, J.Z., Wu, X.R. (1997) *Eng. Fract. Mech*. **57**, 475-491.
6. Beretta, S., Carboni, M. (2005) *Eng. Fract. Mech*. **72**, 1222-1237.
7. Roychowdhury, S., Dodds, R.H., Jr. (2003) *Eng. Fract. Mech*. **70**, 2363-2383.
8. Solanki, K., Daniewicz, S.R. and Newman, J.C., Jr. (2004) *Eng. Fract. Mech*. **71**, 149-171.
9. Solanki, K., Daniewicz, S.R. and Newman, J.C., Jr. (2004) *Eng. Fract. Mech*. **71**, 1165-1175.
10. Toribio, J., Kharin, V. (2009) *Int. J. Solids Struct*. **46**, 1937–1952.
11. Luke, M., Varfolomeev, I., Lütkepohl, K. and Esderts, A. (2009). In *Proc. 2nd Int. Conf. on Material and Component Performance under Variable Amplitude Loading*, Darmstadt, Germany, pp. 259-268.
12. Varfolomeev, I., Luke, M. and Burdack, M. (2009). In: *Damage Tolerance for Railway Axles*, ESIS Workshop, 13-14 Oct. 2008, Milano, paper submitted to *Eng. Fract. Mech.*
13. ABAQUS Standard, Version 6.7, User's Manual, Dassault Systèmes, 2007
14. Traupe, M., Meinen, H., Zenner, H. (2004) *Sichere und wirtschaftliche Auslegung von Eisenbahnfahrwerken*, Abschlussbericht, Clausthal (in German)
15. Fett, T., Munz, D. (1997). *Stress Intensity Factors and Weight Functions*, Computational Mechanics Publications, Southampton UK, Boston USA, 1997